

Optical emission spectroscopy and modeling of DC CO₂-N₂-He mixture plasma

F. Castillo, H. Martínez, O. Flores and C. Cisneros

*Laboratorio de Espectroscopia, Instituto de Ciencias Físicas, Universidad Nacional Autónoma de México,
Apatado Postal 48-3, 62251, Cuernavaca, Morelos, México,
e-mails: ciro@icf.unam.mx; hm@fis.unam.mx; osvaldo@icf.unam.mx; carmen@icf.unam.mx*

P. G. Reyes

*Laboratorio de Física Avanzada, Facultad de Ciencias, Universidad Autónoma del Estado de México,
Instituto Literario 100, Col. Centro, 50000, Toluca, Estado de México, México,
e-mail: pgr.uaemex@gmail.com*

J. Vergara, C. Torres and A. Torres

*Universidad Autónoma del Estado de Morelos,
62715, Morelos, México,
e-mail: vergara@uaem.mx; cetose@gmail.com; alvaro.torres@uaem.mx*

Received 28 June 2024; accepted 5 November 2024

In this study, a direct current carbon dioxide-helium-nitrogen CO₂-N₂-He mixture plasma was studied to evaluate its dependence on pressure. Optical emission spectroscopy (OES), and a Langmuir probe analysis were used to characterize the plasma. The ion number density and electron temperature were determined by a dual Langmuir probe; both values exhibited a slight dependence on the pressure. The species observed via OES exhibited a slight dependence on pressure, and the results were in good agreement with the behavior of the electron temperature and ion density measurements. The N₂/N₂⁺, N/N₂, and N/N₂⁺ ratios as a function of pressure (obtained via OES measurements) were quantitatively correlated with the electron impact excitation and dissociation cross sections ratios. The carbon monoxide/oxygen CO/O₂ ratio as a function of pressure (obtained via OES) indicated that more CO than O₂ was produced, which corresponded with the most important process pertaining to CO₂ splitting. This paper also presents the calculated electron transport coefficients, rate coefficients, electron energy distribution functions, and electron temperatures to support the trends observed during the experiment using *BOLSIG+*, a two-term Boltzmann solver. The rate coefficient due to excitation of the CO₂, N₂, and He obtained by *BOLSIG+* are in good agreement with the present OES observation.

Keywords: OES; glow discharge; Langmuir probe; electron energy distribution function.

DOI: <https://doi.org/10.31349/RevMexFis.71.031501>

1. Introduction

Plasmas that are in part composed of CO₂ and N₂ are extensively applied in the development of high power lasers; the fractional ionization in the discharge may become sufficiently large to allow electron-electron and electron-ion collisions to significantly modify the discharge-transport coefficients. In addition, there are several important applications [1,2] such as plasma sterilization and damage of cancer cells. However, many plasma studies have focused on the possibility of decomposing CO₂; CO₂ is a byproduct of industrial and energy plants, and it contributes to high levels of greenhouse gas emission [3]. The above mentioned studies have clearly shown that CO₂ can be efficiently decomposed into CO and O₂ by non-thermal plasma [4]. In addition, the efficiency of the decomposition process can be altered using mixtures of CO₂ with other gases, which allows to generate additional species of industrial interest [5]. Although the application of DC discharges in pure molecular gases and their mixtures has been increasing in recent years, the full quantitative understanding of the chemistry of such systems

has not yet been attained. Numerous plasma systems have been applied to CO₂ dissociation studies [6-8]. Due to competition from the upstream dissociated CO and O₂ plasma back-reaction, high energy efficiency was only seen at low conversion rates. Due to this phenomenon, there are strict requirements on how well the discharge products-primarily CO from O₂-are separated downstream of the plasma. This lack of understanding is attributed to the absence of reliable data for many physical-chemical reactions and surface processes. In addition, owing to potential technological applications, the investigation of low-pressure plasma in an N₂ glow discharge at pressures of 1-5 Torr for a gas mixture of CO₂-N₂-He has been conducted. In previous studies [9-11], we performed an experimental characterization of DC He-N₂, Ar-CO₂, and CO₂-He/Ar plasma mixtures using optical emission spectroscopy (OES) and mass spectrometry (MS). The objective of this study is to acquire additional knowledge on the chemical products that are formed in a CO₂/N₂/He glow discharge mixture using OES. Both electron temperatures and ion densities were determined with a Langmuir dual probe to characterize the glow discharge mixture. The mea-

measurements were carried out at the pressure of 1.0-5.0 Torr. Also, theoretical calculations have revealed that CO₂/N₂/He mixture is not available until now. To get better understanding and theoretical insights of the present experiment, we use the two term Boltzman solver BOLSIG+ to determine electron transport rate coefficients of the CO₂/N₂/He discharge mixture. Electron transport coefficients and rate coefficients have been discussed from the physical point of view. We examine the behavior of the mean electron energy as a function of the pressure.

2. Experimental setup

The experimental apparatus and technique to generate the DC plasma was recently reported [11] [see Fig. 1a)]. A description is given here. The reactor chamber is coupled with a dual Langmuir probe, and OES diagnostic systems. The reactor included two parallel-plate electrodes with a diameter of 30 mm and a 10 mm separation (d), which were placed in the center of the chamber. The lower electrode and the discharge chamber were grounded, while a negative DC voltage was applied to the upper electrode to generate a glow discharge.

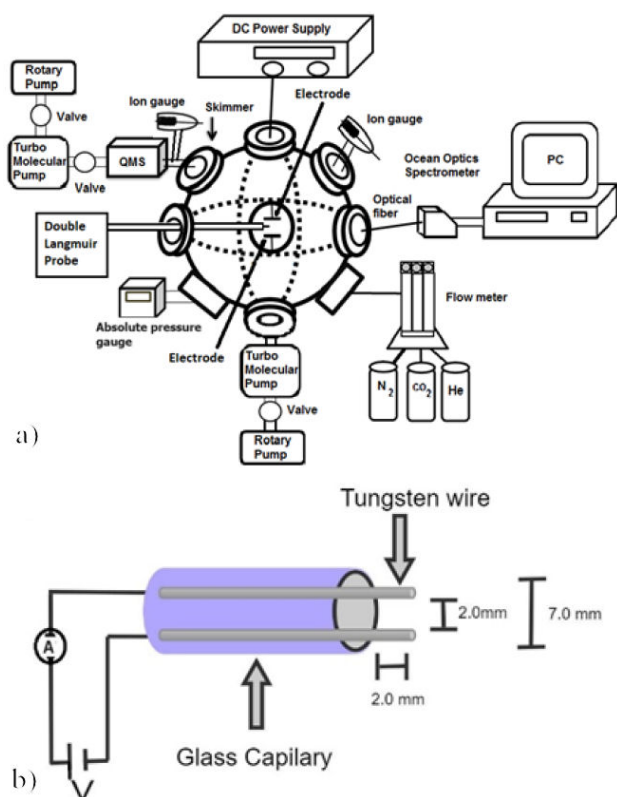
Before each series of measurements, the chamber was evacuated to a base pressure of approximately 10^{-6} Torr using a turbo molecular pump (TMP) (Varian D5302) to ensure a high level of reproducibility. After obtaining the base pressure, the TMP was turned off, and the gases (*i.e.*, CO₂-N₂-He

FIGURE 1. a) Schematic of experimental setup, b) Drawing of dual Langmuir probe.

in the proportion of 5 : 6 : 39 (Praxair 99.99%) were dispersed into the discharge chamber through a continuous dynamic flow of admixture gas in the system through Matheson flow meter model FM1000. The flow rate of admixture gas was 1.8 lmin^{-1} . Next, a gate valve leading to the TMP was partially opened to create a constant flow environment at a given total pressure. A constant current of 10 mA was maintained using a ballast resistance ($R = 200 \Omega$) by changing the power supply voltage. The applied voltage was between 755 and 900 V.

A quartz window was installed to facilitate the monitoring of the active species generated in the glow discharge via OES. An optical fiber located perpendicular to the cylindrical axis of the discharge was used to collect the emitted light of the discharge. A spectrometer (Ocean Optics, model HR2000CG-UV-NIR), which was operated in the spectral range of 200-1,100 nm with a step of 0.35 nm and an optical resolution of 1.0-nm full width at half maximum, was used to obtain the required data. The spectrometer consisted of an OFLV-200-1100 order-sorting filter, which was installed to eliminate any second and third diffraction orders, and a Sony ILX511B linear silicon charge-coupled device (CCD) array (2,048 individual pixels with a pixel size of $14 \times 200 \mu\text{m}$ and a sensitivity of 75 photons/count at 400 nm). The low noise level (250:1 signal-to-noise ratio at full signal) of the CCD allowed for the use of long integration times (resolution times of between 1 ms and 20 s), which are suitable for the detection of extremely low emission intensities, with the spectral data obtained using a 9 s integration time. The spectral range of the OES system was calibrated using an Ar calibration source (Ocean Optics Inc.), while the spectral response was measured using a reference light source (a deuterium lamp for ultraviolet light and an Ocean Optics LS-1-CAL for visible and infrared light). All wavelengths and line intensities were corrected according to the spectral response of the CCD spectrometer and calibrated for the entire wavelength range.

A dual Langmuir probe [Fig. 1b)] is generally used when dealing with an electrode less discharge or when a reference potential is not well defined. Dual probes are inherently advantageous compared with single probes in terms of preventing plasma disturbance since only small currents are drawn from the plasma [10]; the current is limited by the ion saturation current, which is certain orders of magnitude lower than the electron saturation current. In this study, the dual-probe system was electrically floated; therefore, it was less dependent on any potential plasma fluctuations. The dual Langmuir probe consisted of two tungsten wires (radius = 0.25 mm) inserted inside a glass capillary tube with a hole diameter of 7.0 mm; both wires were shielded separately inside the capillary using plastic insulating cylinders. The wire tips were extended 2.0 mm beyond the glass capillary to form active probe tips, with a gap of 2.0 mm between them. The inside bore of the glass capillary was enlarged at the probe end to form a cavity to prevent metal deposits from forming on



the glass, which increased the probe area. The end of the glass capillary was welded with insulating epoxy while excluding the wire tips. The probe was aligned perpendicular to the cylindrical axis of the discharge. The applied voltage to the probe was scanned manually from +30 to -30 V and vice versa using a regulated DC power supply. The probe's current was monitored using a multi-meter (Agilent 34401A: 0.01% accuracy, maximum resolution of 10 nA). The scanning time for one current-voltage (I-V) curve was 2 min. In consideration of any sputtering or contamination of the probe tips, the total measurement time for one probe was restricted to approximately 5-6 h. The final I-V curves were obtained from the average of six data scans at each probe voltage.

3. Results

In this study, the following plasma conditions were used: voltage = 755-900 V, electrode gap (d) = 10 mm, and pressure = 1.0-5.0 Torr. Considering the pressure range of the present work, 1.0 Torr to 5.0 Torr, it was calculated a neutral gas density (N) between $2.41 \times 10^{16} \text{ cm}^{-3}$ (1.0 Torr) and $1.20 \times 10^{17} \text{ cm}^{-3}$ (5.0 Torr) assuming a gas temperature of $T_g = 300 \text{ K}$. Taking into account the ion density n_i of approximately $9.27 \times 10^{10} \text{ cm}^{-3}$ obtained from the probe measurements (Sec. 3.1), an ionization degree (n_i/N) of 10^{-6} was estimated. Given that the ionization degree was $< 10^{-4}$, electron-electron interactions may be neglected [13]. Also, the Debye length (λ_D) for the plasma can be determined using the probe measurements (T_e and n_i), being estimated between 0.049 and 0.052 mm; this value was small compared with the probe radius of 0.25 mm (*i.e.*, $r_p/\lambda_D = 5$), considering the Langmuir probe data reported in Ref. [14] in which the authors stated that the limit of a thin sheath is not reached at $r_p/\lambda_D \leq 50$. So, in the present experiment there is a collision during a sheath transit. In addition, based on the good agreement observed in our previous study [9-11], it can be stated that the reported values were a good approximation of the transition sheath region [15-16].

3.1. Electron temperature and ion density measurement

In this study, $r_p > \lambda_D$, the mean free distance (λ_{ni}) of the ion-neutral collisions varied from 0.056 to 0.060 mm (considering N₂ as neutral), and the sheath thickness was in the range of 0.049-0.052 mm, which is lower than the mean free path. Therefore, the influence of the ion-neutral collision can be neglected. In this case, the probe current (I) as a function of voltage (V) is given by [15-16]

$$I = I_{\infty} \tanh\left(\frac{eV}{2kT_e}\right). \quad (1)$$

The saturation current (I_{∞}) is dependent on ion density (n_i), electron temperature (T_e) and probe area ($A = 3.93 \times 10^{-3} \text{ cm}^2$) as follows:

$$I_{\infty} = Aen_i \left(\frac{kT_e}{2\pi n_i}\right)^{1/2}. \quad (2)$$

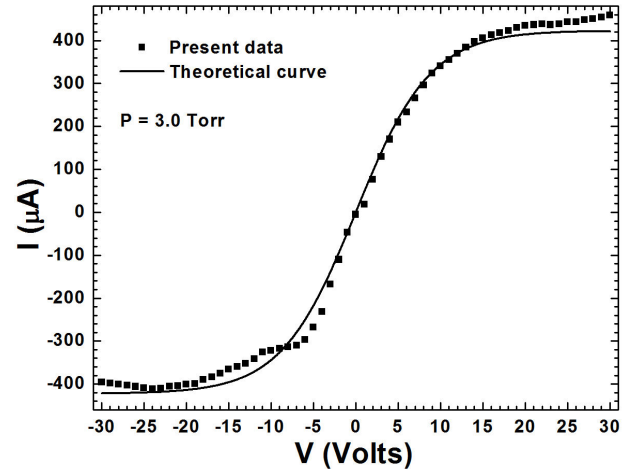


FIGURE 2. Characteristic I-V curve of the double Langmuir probe at 3.0 Torr. (P = pressure).

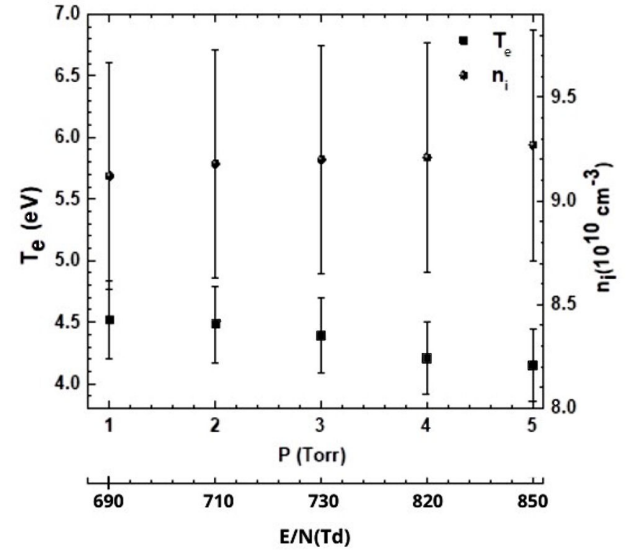


FIGURE 3. Electron temperature and ion density as a function of pressure. ■ T_e ; • n_i .

Figure 2 shows an example of the characteristic I-V curves of the dual Langmuir probe at 3.0 Torr. The theoretical curve (solid line) fitted sufficiently well with the measured data, with a correlation coefficient of 0.985. The different behavior in the saturation region of the characteristic I-V curve may have been due to the sheath expansion effect, or a finite probe used in this study, which could affect the collection of plasma particles. Also, it may be attributed to imperfect probe measurement method and system used in the experiment.

The n_i values were determined from the characteristic I-V curves [10,16] in the ion saturation region using Eq. (1), and the respective T_e were calculated using Eq. (2). The estimated errors of the electron temperature and ion density measurements were 7% and 6%, respectively. (see Fig. 3).

Here, T_e is constant between experimental errors as a function of pressure studied in the present work, while the n_i remained largely constant in the evaluated pressure range. Possibly, this was because the constant behavior of the ionization, recombination, charge exchange, momentum transfer and elastic collision processes in the present pressure range, as can be seen in Sec. 4.

The behaviors of T_e and n_i were qualitatively in good agreement with those reported in Ref. [17], that used almost the same ratio (CO₂-N₂-He) (1 : 1 : 8) within the pressure range used in this study.

3.2. Optical emission measurements

Figure 4 shows the typical OES results for the CO₂-N₂-He glow discharge plasma in the spectral emission range of 200-1,100 nm at 3.0 Torr. Only the most intense spectral lines and bands of the plasma in the 200-1,100 range are quoted [18]. A zoom on region 200-500 nm from Fig. 4 is displayed in Fig. 5. Figures 4 to 6 represent the results of five OES measurements and the overall variations in the intensity and ratios was found to be 10%, 10% and 12%, respectively.

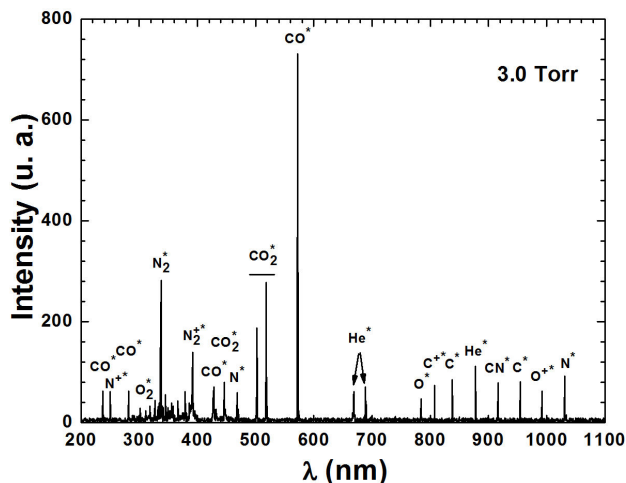


FIGURE 4. Details of Fig. 5 at short wavelength.

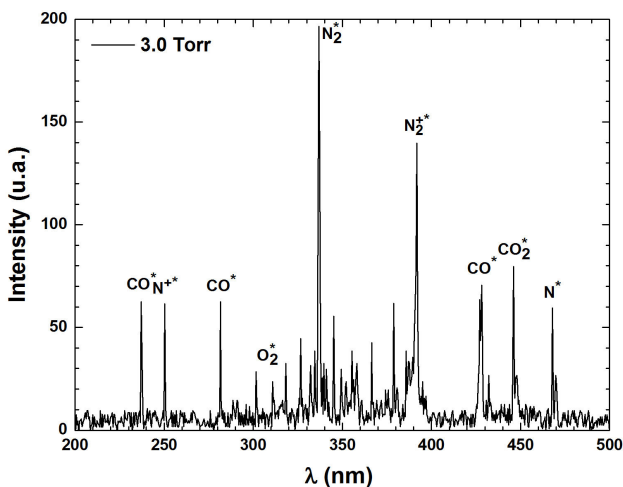


FIGURE 5. Zoom of OES spectra of Fig. 4.

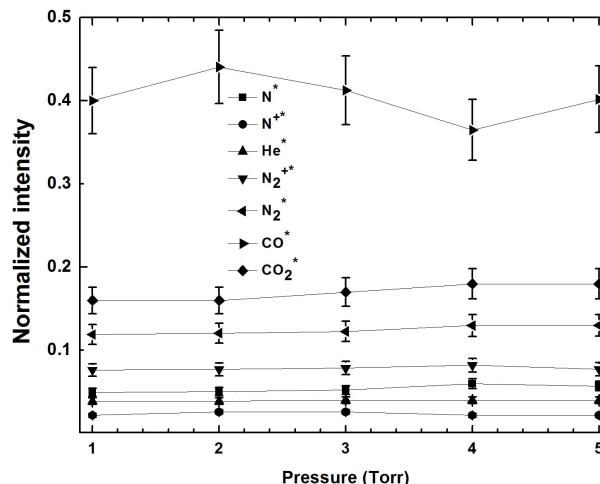


FIGURE 6. Normalized intensity of principal peaks of the mixture as a function of the pressure for: ■ N^+ (1358.13 nm); ● N^{+*} (406.70 nm); ▲ He^* (501.21 nm); ▼ N_2^{+*} (390.87 nm); ◆ CO_2^* (517.12 nm); ◀ N_2^* (687.91 nm); ▶ CO^* (570.99 nm).

The intensity of the O₂^{*}, CN₂^{*}, O^{*}, CN^{*}, C^{*} and N^{*} species remained almost constant in the adopted pressure range of 1.0-5.0 Torr (not shown in Fig. 4 for clarity).

He^{*}, N₂^{*}, and CO₂^{*} matched the strongest lines and bands, whereas C^{*}, N^{*}, O^{*}, and O₂^{*} matched the weakest lines and bands. The examination of the discharge's negative glow region was made possible by this observation. The observed species, namely O₂^{*}, N₂⁺, He^{*}, CO₂^{*}, CO^{*}, N₂^{*}, O^{*}, CN^{*}, C^{*}, C⁺, O⁺, N^{*}, and N⁺, were expected since the primary collision processes were ionization and electron impact excitation. The threshold energies for the ionization and excitation of He were 24.59 and 19.8 eV, respectively; for CO₂, the thresholds were significantly lower at 13.77 eV for ionization, 6.23 eV for electronic excitation, 5.52 eV for dissociation, and only 0.08 eV for vibrational excitation to the lowest vibrational energy. Similarly, for N₂, the thresholds were 15.57 eV for ionization, 6.3 eV for electronic excitation, and 9.77 eV for dissociation. These findings provided an explanation for the behavior that was seen in Fig. 4. In particular, the evolution of each component was analyzed as a function of pressure using the normalized intensities ($I_x/\sum I_x$) to ascertain the impact of the intensity variation of particular species as a function of pressure. The peak value of each specie x is indicated by the line intensity (I_x).

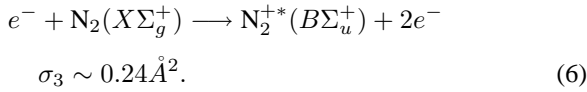
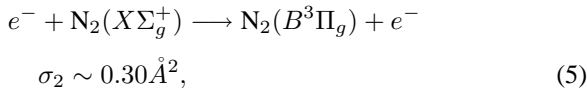
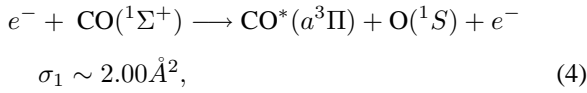
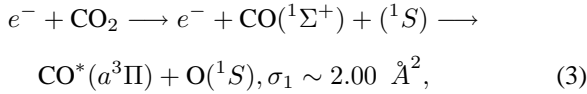
Figure 6 shows the pressure dependence of the normalized intensities of the N₂⁺ (390.87 nm), He^{*} (686.70 nm), CO₂^{*} (517.12 nm), CO^{*} (570.99 nm), and N₂^{*} (638.54 nm) emission lines and bands. Here, the intensity of the CO^{*} species was the strongest (5.52 eV for dissociation) compared with N₂ and He due to the dissociation energy of CO (5.52 eV), which was lower than the excitation energies of N₂ (6.3 eV) and He (19.8 eV).

Table I displays the normalized intensity of CO^{*}, N₂^{*}, N₂⁺ and He^{*} as a function of pressure.

TABLE I. Normalized intensity of CO*, N₂^{*}, N₂^{+*} and He* as a function of pressure.

Pressure (Torr)	CO ₂ [*]	N ₂ [*]	N ₂ ^{+*}	CO ₂ [*]	He*
1.0	0.40	0.12	0.07	0.16	0.04
2.0	0.44	0.12	0.08	0.16	0.04
3.0	0.41	0.12	0.08	0.17	0.04
4.0	0.37	0.13	0.08	0.18	0.04
5.0	0.40	0.13	0.08	0.18	0.04

The three principal processes observed by OES were [19-22]:



The behavior observed in Fig. 6 and Table I are qualitatively correlated with the cross sections of these reaction, that is, $\sigma_1 > \sigma_2 > \sigma_3$ [19-21].

Figure 7 shows the $[\text{N}_2^*/\text{N}_2^{+*}]$, $[\text{CO}^*/\text{N}_2^*]$, and $[\text{CO}^*/\text{N}_2^{+*}]$ ratios as a function of pressure. Here, the three ratios obtained via OES measurements were approximately 1.55, 3.33, and 5.00, respectively, which only qualitatively correlated with the ratio of effective cross sections of the reaction 4, 5 and 6 and implies that in the adopted pressure range, the three processes made the same contribution to the discharge.

Other processes may be contributed to the species intensities observed in Fig. 6. For example, Penning ionization reaction. Nevertheless, the Penning reaction contribution could be estimated from the rate coefficients [23]. The reaction rate for N₂⁺ from the Penning ionization coming from He*–CO₂ and He*–N₂, which could have been mainly in the N₂⁺(B) state, was approximately $1.0 \times 10^{-10} \text{ cm}^3\text{s}^{-1}$ [23,24], while the charge transfer (CT) reaction rates (He⁺+N₂ → N₂⁺+He and He⁺+CO₂⁺ → CO₂⁺+He) [25-27] were approximately $1.3 \times 10^{-9} \text{ cm}^3\text{s}^{-1}$. Given that, as noted, the CT rate coefficient was one order of magnitude higher than the Penning ionization rate coefficient, the CT reaction was mainly responsible for N₂^{+*} with a reaction rate of approximately $1.0 \times 10^{-9} \text{ cm}^3\text{s}^{-1}$. Similarly, the CT reaction was the main reaction that led to N* and N⁺, with a rate of $0.6 \times 10^{-9} \text{ cm}^3\text{s}^{-1}$, resulting in a rate coefficient ratio for

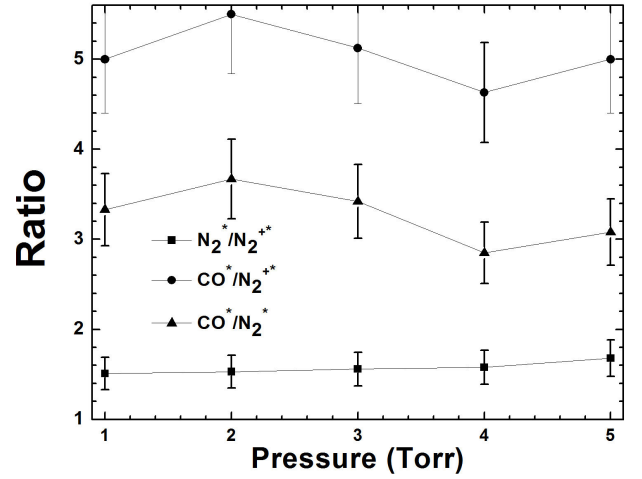


FIGURE 7. $[\text{N}_2^*/\text{N}_2^{+*}]$, $[\text{CO}^*/\text{N}_2^{+*}]$, and $[\text{CO}^*/\text{N}_2^*]$ ratios as a function of the pressure.

$\text{N}_2^+ / (\text{N}^+ + \text{N})$ of 1.7, which was higher than our experimental ratio of 1.07. The differences in the experimental and model data may have been because the model data were obtained at atmospheric pressure and a considerably higher discharge power [25].

As Fig. 7 shows, the $\text{N}^*/\text{N}_2^{+*}$ ratio was approximately 0.7, while the same ratio was estimated to be approximately 0.13 via the theoretical model. Here, it can be assumed that the model [23] did not consider all the possible reaction channels that lead to the production of N*. Additionally, it was also observed that $\text{N}^{+*}/\text{N}_2^{+*}$ had a value of approximately 0.3, while the theoretical model [23] returned a considerably lower value of 0.13. Here, a similar argument to that applied for N/N₂ could be used to explain the difference. That is in good agreement with Ref. [28] that states that the Penning ionization is likely to be the excitation source of N* at low N₂ partial pressure.

Some processes have been mentioned, but there is a process that does not necessary lead to dissociation and chemical decomposition, that is quenching. Direct electron impact ionization of CO₂ and N₂ dominates ion production, two-step ionization of N₂ may be important in some circumstances. This additional source of electrons will most likely involve the metastable N₂ ($A^3\Sigma_u^+$) state which is efficiently excited by direct electron impact and by cascading from higher-lying N₂ electronic levels [29]. This state has a 1.36-sec spontaneous lifetime [30] and, interestingly, is not quenched by collisions with He, N₂, or CO₂ [31,32]. However, several species produced in the discharge including CO, O, and NO_x are very effective to quenching the N₂ ($A^3\Sigma_u^+$) state [31,32]. Also, the ionization cross section for the metastable state is one hundred times that of the ground state [33]. So, two-step ionization of N₂ may contribute significantly to the over-all ionization rate of the discharge if the mixture residence time is 10⁻² sec or less. In the same way, He substantially decreases the relaxation time (by more than a factor of five), probably through a nonradiative CO₂-He collision process

[34]. Therefore, in the present experiment the quenching process could be neglected, despite the pressure change from 1.0 to 5.0 Torr.

Overall, the constant behaviors of the lines and bands observed via OES (Figs. 6 and 7) were consistent with the T_e and n_i results, which exhibited a constant values as a function of pressure.

To explain the obtained OES, it is necessary to consider the possible kinetics for the generation and destruction of the active species (*e.g.*, CO_2 , O_2 , CO , O , N_2 , N , C , and He); this encompasses the processes of electron impact excitation, ionization, and dissociation as well as chemical and decomposition reactions. In fact, the principal processes involved in the CO_2 – N_2 – He plasma discharge were the electron impact excitation of CO_2 , N_2 , and He and the electron impact ionization of N_2 and CO_2 into the upper states, which decayed by emitting photons of different wavelengths. In this study, these processes were recorded and analyzed using the OES technique to identify the different reactive species produced. Electron attachment and electron-ion recombination involving negative ions are also important, and these processes are discussed in Refs. [35] and [36]. Therefore, as observed in the present study, these reactions result in the production of CO_2^* , O_2^* , CO^* , O^* , and He^* .

It was observed (Fig. 4) that the intensity of the O^* specie that potentially correlated with the CO molecule via electron impact dissociation ($e^- + \text{CO}_2 \rightarrow \text{CO} + \text{O}^* + e^-$) was higher than that of the O_2^* species, which was in line with the essential process pertaining to CO_2 splitting [37-39].

4. Reaction rates simulation

For a better understanding on the electron impact reactions rate (excitation, vibrational, dissociation and ionization) in the present investigation, plasma kinetics calculation was done using the numerical Boltzmann equation solver, *BOLSIG+* [40]. The electron reactions rate depends on the reduced electric field (E/N), where $E = V/d$ is the electric field and N is the gas particle number density. For the electron and CO_2 collision cross section, 13 reactions from the Morgan database were used [41], involving electron attachment, excitation, and ionization. For the electron and He collision cross section [42], effective (momentum), excitation, and ionization reactions were used. Finally, for N_2 , 25 reactions were considered [43,44], including electron impact elastic, excitation, and ionization cross sections.

Considering the present experimental condition, *i.e.*, $E/N = 690 - 850 \text{ Td}$ ($1\text{Td} = 10^{-17} \text{ Vcm}^2$), the transport coefficient obtained via *BOLSIG+* was divided by the total gas density N to obtain reduced coefficients that were independent of N .

Figure 8 presents the total collision, the effective momentum transfer in the electron-neutral collision, the electron-ion collision, the total ionization, and the total attachment frequencies. The effective momentum transfer in the electron-neutral and total collision frequencies were the most impor-

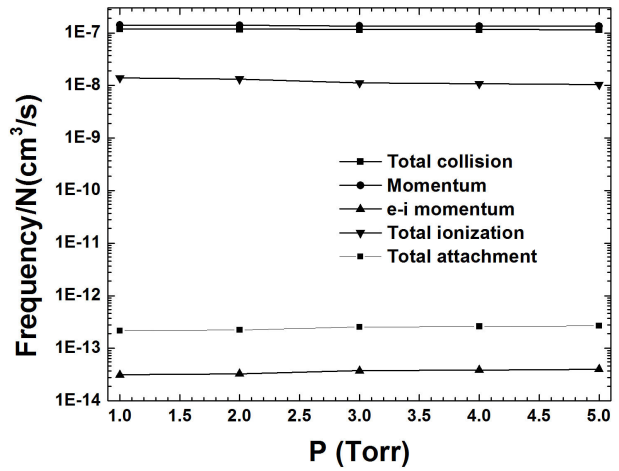


FIGURE 8 Total collision, momentum, electron-ion momentum, total ionization, and total attachment frequencies in relation to the pressure.

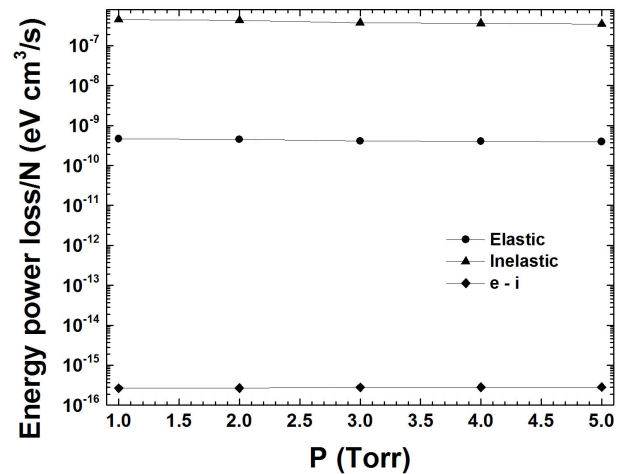


FIGURE 9. Energy power loss rate of the elastic, inelastic, and electron-ion collisions as a function of pressure.

tant and were one order of magnitude larger than the total ionization frequency and six and four orders of magnitude larger than the total attachment and electron-ion momentum frequencies, respectively. The momentum, total collision, and ionization frequencies exhibited a slightly increasing trend as a function of the Pressure P (or decreasing reduced electric field E/N), while the total attachment and electron-ion frequencies exhibited a slightly decreasing trend. The slightly increasing behavior in the total collision frequency provided less time for the electrons to gain energy from the electric field, resulting in a constant value of T_e , as a function of the pressure studied in present work, which agreed with the corresponding experimental results (Fig. 3).

The energy power loss rates due to elastic, electron-ion, and inelastic collisions are presented in Fig. 9, where all of the factors demonstrate almost constant behavior. The most important contribution was the energy loss due to inelastic

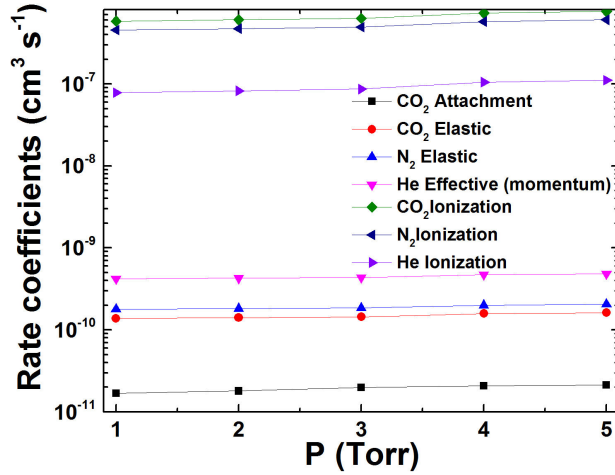


FIGURE 10. Rate coefficients due to the elastic, attachment, effective momentum, and ionization of the N₂, CO₂, and He species as a function of pressure.

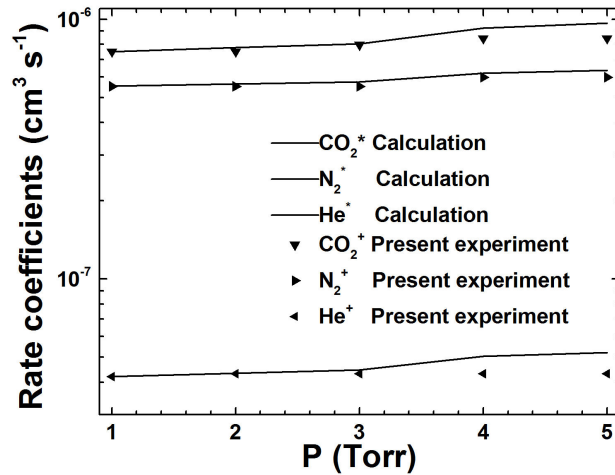


FIGURE 11. Rate coefficients due to the excitation of the N₂, CO₂, and He species as a function of pressure.

collisions, which agreed with the corresponding experimental data and indicated the presence of species formed due to excitation, ionization, and dissociation of the gas phase via electron impact collisions. The contribution of the elastic and electron-ion collisions were less important because it was almost three and nine orders of magnitude less than the total energy loss rate due to the inelastic collisions, respectively, which agree with the present experimental results where the three principal processes were the inelastic reactions (3-5).

The rate coefficients due to the ionization, excitation, elastic, attachment, and effective momentum of the N₂, CO₂, and He species are shown in Figs. 10 and 11. The rate coefficients exhibited almost the same trend except for that of He⁺ and CO₂^{*}, which exhibited only a slightly increasing trend. The most important contributions were from CO₂ excitation (0.083-10.50 eV), CO₂ ionization (13.30 eV), N₂ excitation (0.02-13.00 eV), and N₂ ionization (15.60 eV); this represented an order of magnitude higher than He ionization

(24.58 eV) and excitation (19.80) and two orders of magnitude higher than He effective momentum, N₂ elastic, CO₂ elastic, and six orders with CO₂ attachment processes. These theoretical results are in good agreement with the present experimental observations displayed in Fig. 6 and Table I, where it is shown that the contribution of the species follow the trend CO^{*} > N₂^{*} > N₂⁺ > CO₂^{*} > He^{*}.

Also, Fig. 11 displays the present experimental results obtained by OES to compare with the theoretical calculation. The experimental data were normalized to 1 Torr with the results obtained by *BOLSIG+* for comparison. As can be seen from Fig. 11, the rate coefficient due to excitation of the CO₂, N₂, and He obtained by *BOLSIG+* are in good agreement with the present OES observation (Fig. 6).

The electron energy distribution functions (EEDFs) $f(\epsilon)$ was calculated using *BOLSIG+* software and are presented in Fig. 12 as a function of the electron energy (ϵ) at different pressures. Here, the calculated EEDFs present a non-Maxwellian distribution (EEDFs is not a straight line in the logarithmic plot of Fig. 12) for all the P (or E/N) values, and a substantial change is observed between 1.0 and 5.0 Torr (1333.0 – 746.9 Td). This change likely emerged because the energy loss coefficient for N₂ excitation remained constant while the other energy loss coefficients demonstrated an increasing trend, *i.e.*, the CO₂ excitation and ionization processes became more important than the N₂ excitation and ionization processes.

As P was increased (or E/N decreased), the EEDF shifted to a lower energy. The reduction in EEDF could be attributed to the reduced energy exchange between the molecules and electrons. The increase in P (or decreased in E/N) led to a reduction in molecule-electron energy exchange, thereby reducing the energy range. T_e can be calculated as a mean electron temperature from the EEDF curves as

$$T_e = \int_0^{30} \epsilon^{(3/2)} f(\epsilon) d\epsilon. \quad (7)$$

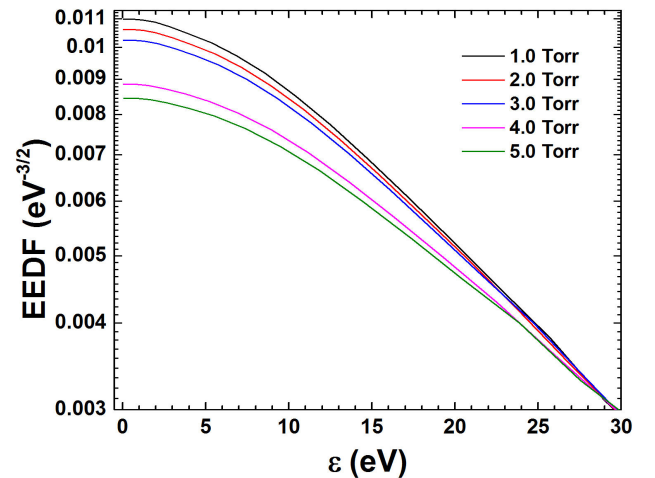


FIGURE 12. Calculated EEDF curves of CO₂-N₂-He plasma mixture as a function of electron energy (ϵ) at several pressures.

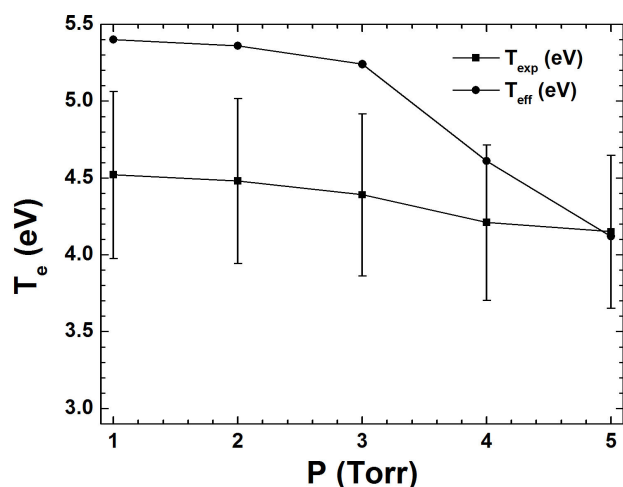


FIGURE 13. Calculated and measured electron temperature of $\text{CO}_2\text{-N}_2\text{-He}$ plasma mixture as a function of pressure.

Figure 13 compares the measured and calculated T_e values, which clearly followed the same trend and shows good agreement between the measured and calculated values. The difference between calculated and experimental T_e values may be attributed to imperfect probe measurement method and system used in the experiment.

5. Conclusions

In this study, a comprehensive electrical and optical characterization of a DC $\text{CO}_2\text{-N}_2\text{-He}$ plasma mixture was conducted. The n_i and T_e values were determined to be approximately $9.25 \times 10^{10} \text{ cm}^{-3}$ and 4.30 eV, respectively, with both remaining almost constant as a function of pressure and

in qualitatively good agreement with the findings reported in previous studies. Furthermore, the OES results were consistent. The species observed via OES were C, C^+ , O, O^+ , N, N^+ , CO, CO_2 , CN, N_2 , N_2^+ , and He, and their behaviors as a function of pressure were consistent with the T_e and n_i measurements in the same pressure range.

The OES measurements indicated that more CO species were produced than O_2 species, which agreed with the most important process pertaining to CO_2 splitting.

The rate coefficients, electron energy distribution function, and T_e were calculated for the $\text{CO}_2\text{-N}_2\text{-He}$ plasma to evaluate the effect of pressure (or E/N) during discharge, while the behavior of the transport parameters on the pressure (or E/N) on the discharge was also clarified. The calculated results agreed with the corresponding experimental results, which indicated that the model provided an accurate representation of the fundamental chemistry involved in the discharge.

The rate coefficient due to excitation of the CO_2 , N_2 , and He obtained by *BOLSIG+* are in good agreement with the present OES observation. We hope that our experimental findings will inspire some theoretical calculation results, which visualized the fundamental chemistry involved in the discharge.

Acknowledgments

The authors are grateful to J. Romero-Vergara, Alfonso Guerrero and H. H. Hinojosa for their technical assistance. This research was funded by DGAPA, grant number IN-102222 and CONACyT, grant numbers 225991 and 268644.

1. L. Chang-jun, X. Gen-hui, W. Timing, Non-thermal plasma approaches in CO_2 utilization. *Fuel Processing Technology*, **58** (1999) 119, [https://doi.org/10.1016/S0378-3820\(98\)00091-5](https://doi.org/10.1016/S0378-3820(98)00091-5).
2. A. S. Chipper, W. Chen, O. Mejlholm, P. Dalgaard and E. Stamate, Atmospheric pressure plasma produced inside a closed package by a dielectric barrier discharge in Ar/CO_2 for bacterial inactivation of biological samples. *Plasma Sources Sci. Technol.*, **20** (2011) 025008, <https://doi.org/10.1088/0963-0252/20/2/025008>.
3. I. Adamovich *et al.*, The 2017 Plasma Roadmap: Low temperature plasma science and technology. *J. Phys. D: Appl. Phys.*, **50** (2017) 32300, <https://doi.org/10.1088/1361-6463/aa76f5>.
4. G. Horvath, J. D. Skalny and N. J. Mason FTIR study of decomposition of carbon dioxide in dc corona discharges. *J. Phys. D: Appl. Phys.*, **41** (2008) 225207, <https://doi.org/10.1088/0022-3727/41/22/225207>.
5. Zhou L. M., Xue B., U. Kogelschatz U. and Eliasson B. Nonequilibrium plasma reforming of greenhouse gases to synthesis gas. *Energy & Fuels*, **12** (1998) 1191, <https://doi.org/10.1021/ef980044h>.
6. N. Lisi, U. Pasqual Laverdura, R. Chierchia, I. Luisetto, and S. Stendardo, A water cooled, high power, dielectric barrier discharge reactor for CO_2 plasma dissociation and valorization studies. *Sci Rep* **13** (2023) 7394, <https://doi.org/10.1038/s41598-023-33241-9>.
7. Y. Xu, Y. Gao, D. K. Xi, L. G. Dou, C. Zhang, B. W. Lu, T. Shao, Spark Discharge Plasma-Enabled CO_2 Conversion Sustained by a Compact, Energy-Efficient, and Low-Cost Power Supply. *Industrial & Engineering Chemistry Research* **62** (2023) 15872, <https://doi.org/10.1021/acs.iecr.3c02393>.
8. S. Renninger, J. Stein, M. Lambarth, and K. P. Birke, An optimized reactor for CO_2 splitting in DC atmospheric pressure discharge. *J. CO₂ Util.* **58** (2022) 101919, <https://doi.org/10.1016/j.jcou.2022.101919>.
9. H. Martínez *et al.*, Study of DC Ar-CO_2 mixture plasma using optical emission spectroscopy and mass spectrometry techniques. *Physics of Plasmas*, **24** (2017) 043508, <https://doi.org/10.1063/1.4979995>.

10. O. Flores, F. Castillo, H. Martínez, M. Villa, S. Villalobos and P. G. Reyes Characterization of direct current He-N₂ mixture plasma using optical emission spectroscopy and mass spectrometry. *Physics of Plasmas*, **21** (2014) 053502, <https://doi.org/10.1063/1.4875343>.
11. P. G. Reyes, C. Torres and H. Martínez, Electron temperature and ion density measurements in a glow discharge of an Ar-N₂ mixture. *Radiation Effects and Defects in Solids*, **169** (2014) 285, <https://doi.org/10.1080/10420150.2013.860975>.
12. B. M. Annaratone, G. F. Counsel, H. Kawano and J. E. Allen, On the use of double probes in RF discharges. *Plasma Sources Sci. Technol.* **1** (1992) 232, <https://doi.org/10.1088/0963-0252/1/4/002>.
13. M. Janda, V. Martisovits M., Morvova, Z. Machala and K. Hensel, Monte Carlo simulations of electron dynamics in N₂/CO₂ mixtures. *Eur. Phys. J. D*, **45** (2007) 309, <https://doi.org/10.1140/epjd/e2007-00254-x>.
14. C. Steinbruche, A new method for analyzing Langmuir probe data and the determination of ion densities and etch yields in an etching plasma. *Journal of Vacuum Science and Technology A* **8** (1990) 1663, <https://doi.org/10.1116/1.576782>.
15. K. U. Riemann, The influence of collisions on the plasma sheath transition. *Physics of Plasmas*, **4** (1997) 4158, <https://doi.org/10.1063/1.872536>.
16. J. D. Swift and M. J. R. M. Schwar, *Electrical Probes for Plasma Diagnostics*. Editorial: Iliffe Books; (American Elsevier, London, New York, 1970).
17. S. Ono and S. Teii, Negative ion formations and their effects on the electron temperature in CO₂-N₂-He mixture gas discharges. *J. Phys. D: Appl. Phys.*, **17** (1984) 1999, <https://doi.org/10.1088/0022-3727/17/10/011>.
18. R. W. B. Pearse and A. G. Gaydon, *The identification of molecular spectra*. Fourth edition. (Chapman and Hall, London, New York, 1976). pp. 397.
19. Y. Itikawa, Cross sections for electron collisions with carbon dioxide, *Journal of phys. Chem. Ref. Data* **31** (2002) 749, <https://doi.org/10.1063/1.1481879>.
20. A. Laricchiuta, L.D. Pietanza, M. Capitelli, and G. Colonna Electron-CO excitation and ionization cross sections for plasma modeling. *Plasma Phys. Control Fusion*, **61** (2019) 014009, <https://doi.org/10.1088/1361-6587/aae16b>.
21. Mi-Y Song, H. Cho, G.P. Karwasz, V. Kokoouline, and J. Tenynson Cross Sections for Electron Collisions with N₂, N₂^{*}, and N₂⁺. *J. Phys. Chem. Ref. Data* **52** (2023) 023104, <https://doi.org/10.1063/5.0150618>.
22. Y. Itikawa, Cross Sections for Electron Collisions with Nitrogen Molecules, *J. Phys. Chem. Ref. Data* **35** (2006) 31, <https://doi.org/10.1063/1.1937426>.
23. G. M. Petrov *et al.*, Numerical Modeling of a He-N₂ Capillary Surface Wave Discharge at Atmospheric Pressure. *Plasma Chemistry and Plasma Processing*, **20** (2000) 183, <https://doi.org/10.1023/A:1007065022725>.
24. M. Tsuji, T. Tanoue, K. Nakano and Y. Nishimura, Decomposition of CO₂ into CO and O in a microwave-excited discharge flow of CO₂/He or CO₂/Ar mixtures. *Chemistry Letters*, **30** (2001) 22, <https://doi.org/10.1246/cl.2001.22>.
25. V. Guerra *et al.*, Time-Dependence of the electron energy distribution function in the nitrogen afterglow. *IEEE Trans. Plasma Sci.* **31** (2003) 542, <https://doi.org/10.1109/TPS.2003.815485>.
26. J. Raud and M. Laan, Positive column of HF discharge in He/N₂ mixture: excitation and ionization mechanisms. *J. Phys. D: Appl. Phys.* **42** (2009) 015205, <https://doi.org/10.1088/0022-3727/42/1/015205>.
27. S. D. Rockwood, Elastic and inelastic cross sections for electron-Hg scattering from Hg transport data. *Phys. Rev. A* **8** (1972) 2348, <https://doi.org/10.1103/PhysRevA.8.2348>.
28. S. De Benedictis, G. Dilecce and M. Simek, Vibrational excitation of N₂⁺ (β , ν) in He-N₂ pulsed RF discharges. *J. Phys. B: at. Mol. Opt.* **27** (1994) 615, <https://doi.org/10.1088/0953-4075/27/3/025>.
29. J. A. Meyer, D. W. Setser and W. G. Clark, Rate constants for quenching of N₂(A³ Σ_u^+) in active nitrogen. *J. Phys. Chem.* **76** (1972) 1, <https://doi.org/10.1021/j100645a001>.
30. R. A. Young, G. Black and T. G. Slanger, Vacuum-ultraviolet photolysis of N₂O. II. deactivation of N₂(A³ Σ_u^+ *rpar; and N₂(B³ Π_g). *J. Chem. Phys.* **50** (1969) 303, <https://doi.org/10.1063/1.1670792>.
31. F. J. Mehr and M. A. Biondi, The dissociative recombination of molecular ions. *Phys. Rev.* **181** (1969) 264, <https://doi.org/10.1103/PhysRev.181.264>.
32. J. T. Moseley, W. Aberth and J. R. Peterson, Two-body mutual neutralization rates of O₂⁺+O⁻, NO⁺+O⁻, and Na⁺+O⁻ obtained with merged beams. *J. Geophys. Res.* **77** (1972) 255, <https://doi.org/10.1029/JA077i001p00255>.
33. W.J. Wiegand and W.L. Nighan Plasma chemistry of CO₂-N₂ discharges. *Appl. Phys. Lett.* **22** (1973) 583, <https://doi.org/10.1063/1.1654516>.
34. P. K. Cheo, Effects of CO₂, He, and N₂ on the lifetimes of the 00⁰1 and 10⁰0 CO₂ laser levels and on pulsed gain at 10.6 μ . *Journal of Applied Physics*. **38** (1967) 3563, <https://doi.org/10.1063/1.1710173>.
35. A. N. Goyette, J. R. Peck, Y. Matsuda, L. W. Anderson, and J. E. Lawler Experimental comparison of rotational and gas kinetic temperatures in N₂ and He-N₂ discharges. *J. Phys. D*, (1998) **31** 1556, <https://doi.org/10.1088/0022-3727/31/13/009>.
36. V. I. Arkhipenko, A. A. Kirillov, L. V. Simonchik, and S. M. Zgirouski, Influence of the nitrogen-helium mixture ratio on parameters of a self-sustained normal dc atmospheric pressure glow discharge. *Plasma Sources Sci. Technol.* **14** (2005) 757, <https://doi.org/10.1088/0963-0252/14/4/015>.
37. S. Ponduri, M. M. Becker, S. Welze, M. C. M. Van de Sanden, D. Loffhagen and R. Engeln Fluid modelling of CO₂ dissociation in a dielectric barrier discharge. *J. Appl. Phys.* **119** (2016) 093301, <https://doi.org/10.1063/1.4941530>.
38. T. Martens, Bogaerts A., Brok W.J.M. and Dijk J. V. The dominant role of impurities in the composition of high pressure noble gas plasmas. *Appl. Phys. Lett.* **92** (2008) 041504, <https://doi.org/10.1063/1.2839613>.

39. T. G. Beuthe and J. S. Chang, Chemical kinetic modelling of non-equilibrium Ar-H₂ thermal plasmas. *Jpn. J. Appl. Phys.* **36** (1997) 4997, <https://doi.org/10.1143/JJAP.38.4576>.
40. G. J. M. Hagelaar and L. C. Pitchford, Solving the Boltzmann equation to obtain electron transport coefficients and rate coefficients for fluid models. *Plasma Source Sci. Technol.* **14** (2005) 722, [10.1088/0963-0252/14/4/011](https://doi.org/10.1088/0963-0252/14/4/011).
41. Morgan database. Retrieved April 12, 2023. <https://www.lxcat.laplace.univtlse.fr>.
42. A.V. Phelps and L.C. Pitchford Anisotropic scattering of electrons by N₂ and its effect on electron transport. *Phys. Rev. A* **31** (1985) 2932, <https://doi.org/10.1103/PhysRevA.31.2932>.
43. SIGLO database. Retrieved April 12, 2023. <https://www.lxcat.laplace.univtlse.fr>.